INSTITUTE OF PHYSICS PUBLISHING JOURNAL OF PHYSICS D: APPLIED PHYSICS

J. Phys. D: Appl. Phys. **37** (2004) 2720–2725 PII: S0022-3727(04)81944-2

Interface properties of iron oxide films

S Jain[1], A O Adeyeye[1,4], S Y Chan[2] and C B Boothroyd[3]

[1] Information Storage Materials Laboratory, Department of Electrical & Computer Engineering, 4 Engineering Drive 3, National University of Singapore, Singapore
[2] Data Storage Institute, DSI Building 5, Engineering Drive 1, Singapore
[3] Institute of Materials Research and Engineering, 3, Research Link, Singapore

E-mail: eleaao@nus.edu.sg (A O Adeyeye)

Received 2 June 2004
Published 15 September 2004
Online at stacks.iop.org/JPhysD/37/2720
doi:10.1088/0022-3727/37/19/016

Abstract

We have investigated in a systematic way the interface properties of Fe_2O_3 grown on different buffer layers using an electron beam deposition technique. For films deposited directly onto Si(001) substrate and on Al buffer layer, we observed the presence of metallic Fe at the Si(001) and Al interfaces, respectively. We also detected the presence of SiO_2 and Al_2O_3 by x-ray photoelectron spectroscopy. For Fe_2O_3 films deposited on Cu buffer layer, however, no other phases were observed at the interface. We explain our results using the enthalpy of formation. The enthalpy of formation of SiO_2 and Al_2O_3 is much lower than that of Fe_2O_3, thus inhibiting the crystalline growth of Fe_2O_3 at the interface. The enthalpy of formation of CuO is, however, greater than that of Fe_2O_3, and thus promoting the growth of Fe_2O_3 to be crystalline. These results were corroborated by our transmission electron microscopy studies.

(Some figures in this article are in colour only in the electronic version)

1. Introduction

Thin iron oxide films have been the subject of many studies due to their interesting magnetic properties. Iron oxide can exhibit several crystal structures and compositions, including wustite (FeO), which has a rocksalt phase, magnetite (Fe_3O_4) and maghemite (γ-Fe_2O_3), which are both cubic spinel phases, and haematite (α-Fe_2O_3), which is a corundum phase [1]. Maghemite is of particular interest because of its application in magnetic recording media [2], pigments [3], catalysts [4] and gas sensitive materials [5]. It has a cubic spinel structure and is known to be a ferrimagnetic with a saturation magnetization of 390 kA m^{-1} [6]. Maghemite is a metastable phase at ambient conditions, and tends to transform to a stable phase of antiferromagnetic haematite (α-Fe_2O_3) when heated above 400°C [7]. It is therefore of great interest to deposit ferrimagnetic maghemite and suppress its transformation to the equilibrium antiferromagnetic haematite structure.

Iron oxide films have been produced using various methods. Tepper and Ross [8] deposited γ-Fe_2O_3 using a pulsed laser deposition technique by ablating a pure α-Fe_2O_3 target. In another work by Ye *et al* [7], γ-Fe_2O_3 was synthesized by the wet chemical method using aqueous $Fe(NO_3)_3$ solution, 2-ethyl hexanol and sorbitan monooleate surfactant.

In this paper, we have studied the growth of Fe_2O_3 on various templates using electron beam deposition. We observed that the crystal structure of Fe_2O_3 depends greatly on the interface properties between Fe_2O_3 and the template on which it is deposited. The main advantage of this method over other techniques is the ability to control the thickness of the film without the presence of reactive ambient gases. The role of surface states in determining the optimum conditions for the deposition of ferrimagnetic Fe_2O_3 on various templates has been investigated. We observed that the enthalpies of formation of various oxides play an important role in determining the crystallinity of Fe_2O_3. For films deposited on Cu buffer layer, we found that the stoichiometry of the Fe_2O_3 is preserved throughout the film thickness. We observed a mixed valence state of iron oxide at the interface when Fe_2O_3 is deposited directly on Si(001) substrate and on Al buffer layer. This was confirmed using x-ray

[4] Author to whom any correspondence should be addressed.

Table 1. Description of various samples used in the experiments.

Sample	Film structure
A	Si(001)/Fe_2O_3 (200 nm)
B	Si(001)/Cu (100 nm)/Fe_2O_3 (200 nm)
C	Si(001)/Cu (100 nm) oxidized in atm./Fe_2O_3 (200 nm)
D	Si(001)/Al (40 nm)/Fe_2O_3 (200 nm)
E	Si(001)/Fe_2O_3 (20 nm)/Cu (5 nm)

photoelectron spectroscopy (XPS) and transmission electron microscopy (TEM).

2. Experimental details

Fe_2O_3 films were deposited using electron beam deposition from a pure Fe_2O_3 target on to Si(001) substrates. The base pressure was maintained at 3×10^{-7} Torr. Prior to deposition, the substrates were ultrasonically cleaned in acetone for 30 min, and were then rinsed in isopropanol. Fe_2O_3 films were grown on various templates as shown in table 1. For all the samples, the substrate temperature was maintained at 50°C during the entire deposition.

XPS was used to determine the relative amounts of Fe and Fe oxides present in the deposited films. XPS depth profile analysis was performed using a Physical Electronics Quantum 2000 Scanning ESCA Microprobe equipped with a monochromatized Al Kα source ($h\nu = 1486.6$ eV). Depth profiles of Fe 2p, O 1s, and Si 2p were acquired for 200 nm Fe_2O_3 films with a pass energy of 93.9 eV at 0.2 eV step size and Ar^+ beam energies of 1 kV rastered over 3 mm × 3 mm with a calibrated sputter rate of 16 Å min^{-1}, calibrated using SiO_2. For the depth profile analysis of the 20 nm Fe_2O_3 films, a beam energy of 500 eV rastered over 2 mm × 2 mm (corresponding to a sputtering rate of 10 Å min^{-1}, calibrated against SiO_2) with Zalar rotation was used. To protect the Fe_2O_3 film from further oxidation while transferring the sample from the deposition chamber to the photoelectron spectrometer, we capped it with 5 nm Cu capping layer. The intensities for all the XPS spectra reported here were normalized for comparison and were calibrated against the C 1s peak (284.8 eV) of adventitious carbon. A 200 μm x-ray beam size was used for all acquisitions at a take-off angle of 45°. It should be noted that preferential sputtering did not occur in our films. The low sputtering energy of 500 eV used throughout the experiment was carefully selected to minimize any preferential sputtering and also to have a sharper interface. TEM study was carried out using a Philips CM300 300 kV field-emission transmission electron microscope to investigate the interfacial reactivity between Fe_2O_3 film and the buffer layer beneath it. We have characterized the magnetic properties of Fe_2O_3 films using a vibrating sample magnetometer. Phase identification and crystal structure of the Fe_2O_3 films were examined by conventional θ–2θ scans of x-ray diffraction (XRD) using a Cu Kα radiation.

3. Discussion

Figure 1(*a*) shows the Fe 2p core level XPS spectra as a function of sputtering time for an Fe_2O_3 film deposited directly on

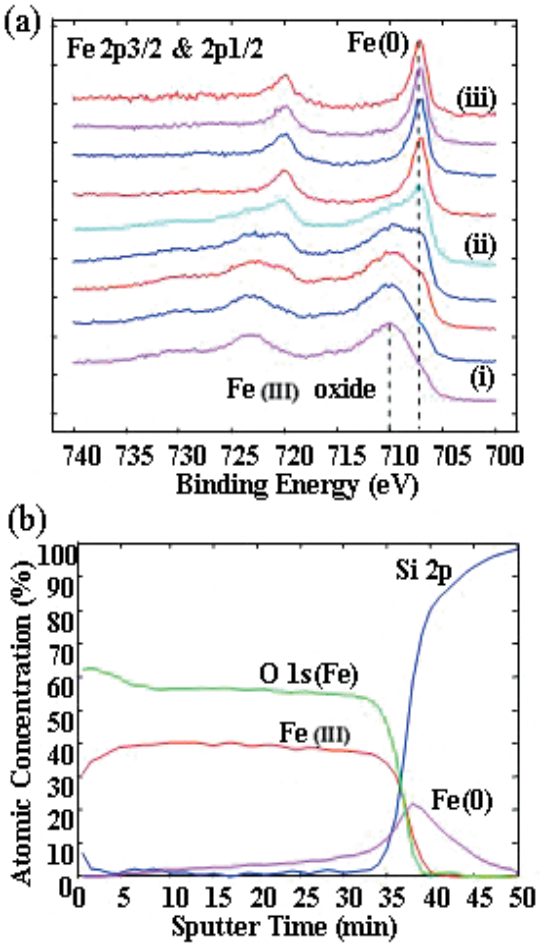

Figure 1. (*a*) XPS core level spectra of Fe 2p3/2 and 2p1/2 for 200 nm Fe_2O_3 deposited directly onto the Si(001) substrate taken on (i) 'as received', (ii) after 35 min sputtering and (iii) after 40 min sputtering during depth profile analysis and (*b*) atomic concentrations of Fe, Fe(III), O 1s, and Si as a function of sputtering time for 200 nm Fe_2O_3 deposited directly onto the Si(001) substrate.

Si(001). We observed that the Fe 2p binding energy from the unsputtered surface is at 710 eV, which is the binding energy associated with Fe(III) oxide. The corresponding O 1s peak has a binding energy of 530 eV. Moreover, no Si peak is detected, confirming that the surface is Fe_2O_3.

After 35 min of sputtering, a small 'shoulder' is observed on the Fe 2p3/2 spectra at a binding energy of about 707 eV (figure 1(*a*)). A similar observation is found for the O 1s peak, where one 'small bump' is seen at a higher binding energy of about 532 eV. In addition to this, a Si signal is also detected, which shows a mixed state containing both elemental silicon (99 eV) and silicon oxide (103 eV). Though the Si(001) substrate was cleaned thoroughly before loading it into the evaporator chamber, there is a possibility of native SiO_2 being present on its surface. However, it should be noted that the Si material would still be very reactive towards oxygen, and will be further oxidized during the deposition of Fe_2O_3. After 40 min of sputtering, no Fe(III) is seen and only metallic Fe(0) is present, as can be seen from figure 1(*a*). We observed a clear and sharp change in the binding energy from Fe(III) to

Fe(0) as we sputtered through the entire depth. Also from the analysis, we found no presence of Fe(II) (even if it was present in trace amounts, it cannot be distinguished easily from Fe(III)). A trace amount of oxygen is still detected at a binding energy of about 532 eV, which is probably attributed to a residue of silicon dioxide. Moreover, as mentioned earlier, the low sputtering energy used in Ar^+ sputtering decreased the possibility of a reduced surface (or preferential sputtering), otherwise we would have not observed a 'pure' Fe(0) peak.

Figure 1(*b*) shows the atomic concentration of these species as a function of sputter time derived from figure 1(*a*) and similar profiles for the other elements. We observed that the concentration of O 1s is constant and decays after 35 min of sputtering as the sputtered surface reaches the Si(001) and Fe_2O_3 interface. The oxides of Fe and Si in this analysis were separated using peak-fitting method. Likewise, the concentration of Fe(III) oxide begins to decrease as it approaches the interface. However, we also observed the significant presence of Fe(0) after 35 min of sputtering, which can be attributed to Fe particles. We can conclude from the XPS spectra in figure 1 that after 35 min of sputtering, the surface is at the boundary between the Fe_2O_3 and a layer containing Fe(0) and silicon oxide. On the other hand, after 40 min of sputtering, the surface is at the interface between Fe(0) and Si(001) substrate.

The presence of Fe(0) can be explained by the fact that during electron beam deposition, a beam of electrons falls on the target material (Fe_2O_3) and decomposes it to Fe and free oxygen. On comparing the enthalpy of formation for Fe(III) oxide and Si(IV) oxide, we noticed that the formation of Si(IV) oxide has a much lower enthalpy energy than the formation of Fe(III) oxide. This suggests that there is a continuous competition at the template interface for oxygen to react and form an oxide. Due to the lower enthalpy of Si(IV) oxide, as can be seen from table 2, free oxygen at the interface readily reacts with Si and forms Si(IV) oxide, leaving behind metallic Fe(0) and hence non-stoichiometric growth of Fe_2O_3.

A similar depth profile analysis was repeated for sample B (Fe_2O_3 deposited on Cu on Si) to study the stoichiometry of the Fe_2O_3 deposited. Figure 2(*a*) shows the Fe 2p core level spectra from similar sputtering intervals to those presented in figure 1(*a*). There is no obvious chemical shift of the Fe 2p peaks during sputtering, indicating that the Fe 2p3/2 binding energy remains constant at about 710 eV, consistent with Fe(III) oxide. The binding energies for its associated O 1s peak, 530 eV, are also consistent with Fe(III) oxide throughout the sputtered depth. Figure 2(*b*) shows the Cu 2p spectra at different time intervals of (i) after 40 min of sputtering from the surface, (ii) after 50 min of sputtering and (iii) after 60 min of sputtering. We clearly observed no shift in the binding energy (932 eV) of the Cu 2p peak throughout its depth. Therefore, no other oxidation state of Cu was observed. Furthermore, we present in figure 2(*c*), the atomic concentration depth profile analysis for sample B. We observed a constant concentration of Fe(III) oxide throughout the film thickness. This suggests that the stoichiometry of the Fe_2O_3 film remains unchanged throughout the 40 min of sputter etching. This observation is in agreement with the theory of surface oxidation, whereby the enthalpy of formation of CuO, as shown in table 2, is much higher than that of Fe(III) oxide. Therefore, at the interface, Fe(III) oxide is formed easily as compared to CuO.

To verify that the growth mechanism of Fe_2O_3 still remains the same, regardless of the presence of native oxides on the layer beneath it, we deposited a Cu buffer layer onto Si(001)

Table 2. Enthalpy energy values for various oxides.

Oxide	Enthalpy (kJ mol^{-1}) [10]
Fe_2O_3	−822.30
SiO_2	−910.70
CuO	−155.00
Al_2O_3	−1674.00

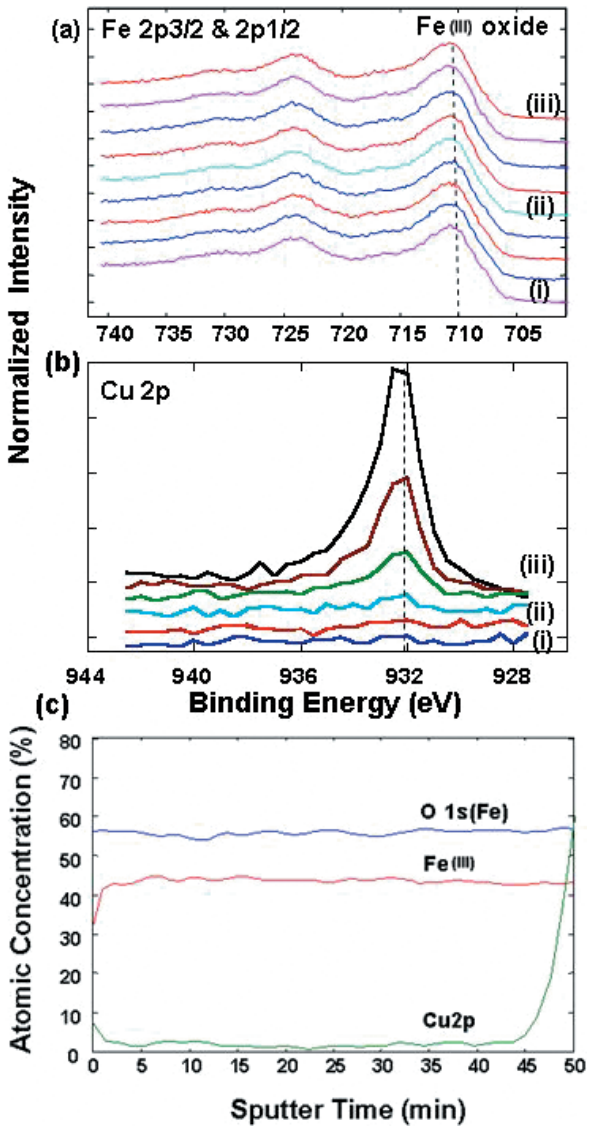

Figure 2. XPS core level spectra of (*a*) Fe 2p3/2 and 2p1/2 for 200 nm Fe_2O_3 deposited on 100 nm Cu buffer layer taken on (i) 'as received', (ii) after 35 min sputtering and (iii) after 40 min sputtering during depth profile analysis; (*b*) Cu 2p taken after (i) 40 min sputtering, (ii) 50 min sputtering and (iii) 60 min sputtering interval from the surface; and (*c*) atomic concentrations for various elements as a function of sputter time.

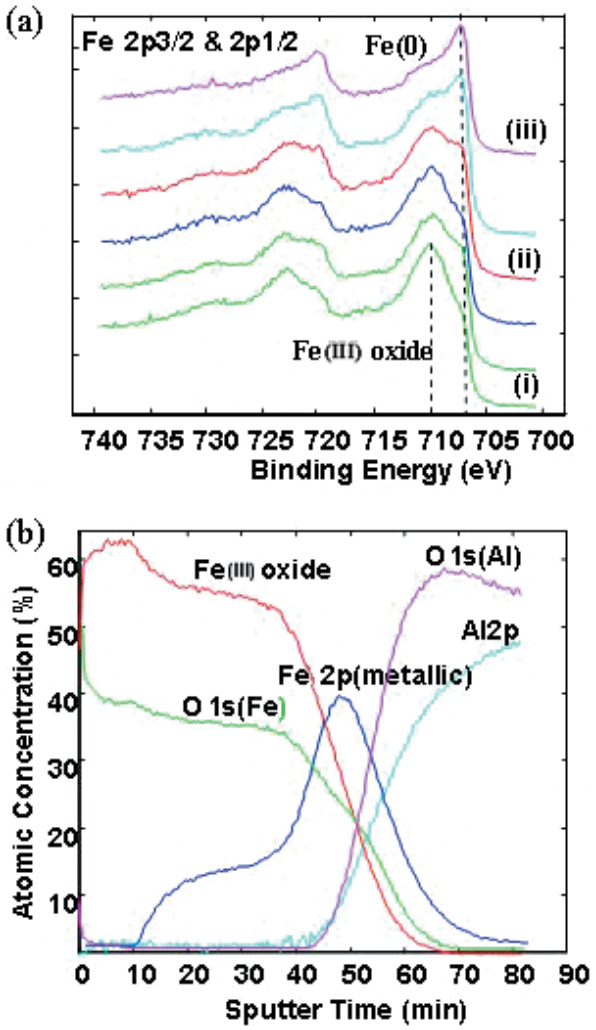

Figure 3. (*a*) XPS core level spectra of Fe 2p3/2 and 2p1/2 for 200 nm Fe_2O_3 deposited on 40 nm Al buffer layer taken on (i) 'as received', (ii) after 35 min sputtering and (iii) after 40 min sputtering during depth profile analysis; and (*b*) atomic concentrations for various elements as a function of sputter time for Fe_2O_3 on Al buffer layer.

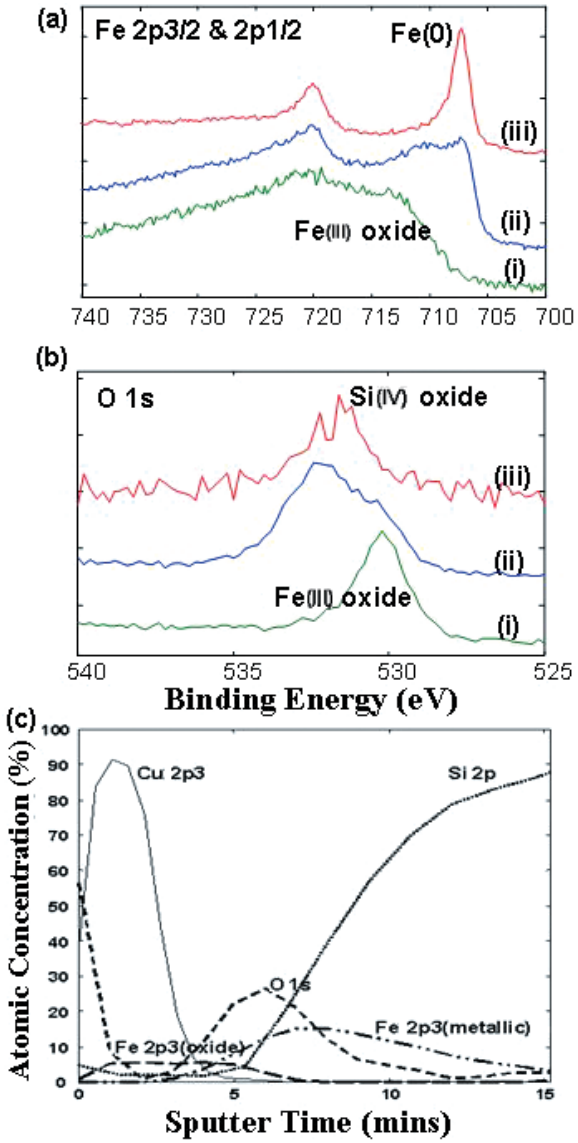

Figure 4. (*a*) Fe 2p; (*b*) O 1s core level XPS spectra as a function of sputtering time shown as (i) 'as received', (ii) after 8.5 min sputtering and (iii) after 15 min sputtering during depth profile analysis from a 20 nm Fe_2O_3 film on a silicon substrate with a 5 nm copper capping layer; and (*c*) shows the corresponding atomic concentration profile for various elements as a function of sputter time.

and then exposed it to the atmosphere so that a thin layer of CuO was formed. The sample was then loaded back into the deposition chamber and 200 nm of Fe_2O_3 was deposited. The XPS depth profile analysis of this sample shows that the stoichiometry of Fe_2O_3 remained unchanged throughout the film thickness. This is in agreement with our argument based on the enthalpy of formation, where the enthalpy energy of CuO is higher than that of Fe(III) oxide. Thus, Cu buffer layer promotes the growth of crystalline Fe_2O_3.

The Fe 2p XPS spectra from the sample consisting of Fe_2O_3 film deposited on an Al buffer layer on Si(001) substrate (sample C) is shown in figure 3(*a*) as a function of sputtering time. We observed a chemical shift in the binding energy from Fe(III) to Fe(0) similar to that seen in figure 1(*a*). Further, figure 3(*b*) shows the atomic concentration profile as a function of sputter time for the same sample. We observed a sharp decay in the Fe(III) oxide and O 1s(Fe) concentrations after 40 min of sputtering, i.e. at the Fe_2O_3/Al interface. This corresponds to a sharp increase in the Fe 2p (metallic) concentration at the interface indicating the presence of metallic Fe. The presence of Al_2O_3 is shown by the sudden increase in the O 1s(Al) concentration after 40 min of sputtering. It should be noted that the O 1s peak for both Fe_2O_3 and Al_2O_3 have close binding energies, around 529–531 eV. It is therefore difficult to separate them. However, the Al 2p peak gives us a clearer clue where there is a distinguishable binding energy between Al(0) and Al(III). From here, we deduced the presence of Al(III) oxide instead of looking at the O 1s peak alone. Moreover, the concentration of Al(III) oxide formed is much greater than the Si(IV) oxide formed shown in figure 1(*b*). From the analysis, we observed that the enthalpy of formation for Al_2O_3 is again lesser than the enthalpy of Fe_2O_3, as shown in

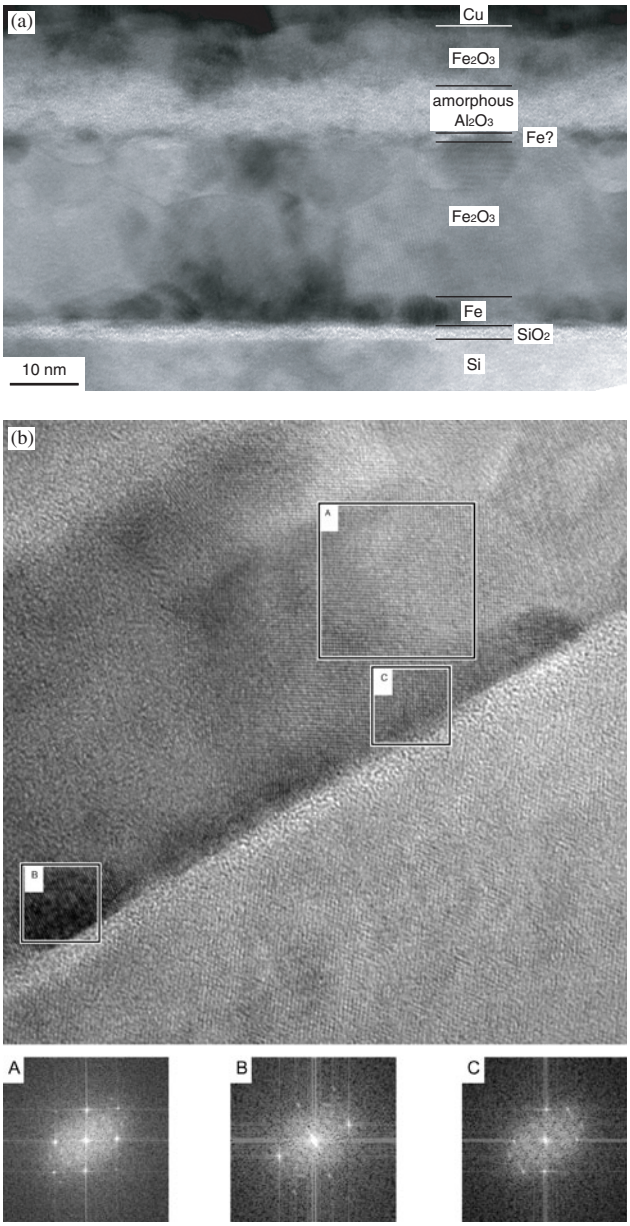

Figure 5. (*a*) Bright field cross-sectional TEM micrograph of sample A showing the presence of Fe particles adjacent to the Si substrate. (*b*) High-resolution image of the interface adjacent to the Si substrate. The three diffractograms at the bottom come from the areas marked by boxes on the image and were used for identification of the crystal structure and zone axis of the grains. They are: A, Fe_2O_3 [$2\bar{5}1$]; B, Fe [001] and C, Fe [110].

table 2. This confirms our argument that the enthalpies of the different oxides play an important role in the stoichiometric growth of Fe_2O_3.

In order to ascertain that the presence of metallic Fe at the interface was due to surface oxidation of the Si substrate by Fe(III) oxide, a 20 nm layer of Fe_2O_3 was deposited directly onto Si(001) without any Cu buffer layer. The film was then capped with 5 nm of Cu to prevent further oxidation. This sample was then analysed by XPS depth profiling, as shown in figure 4. As expected, the surface shows a relatively weak intensity of Fe(III) oxide before sputtering. After 8.5 min of sputtering (about 8 nm, calibrated using SiO_2), the metallic Fe 2p3/2 peak at 707 eV starts to appear on the right shoulder of the main Fe(III) oxide peak (figure 4(*a*)). In addition, a chemical shift for O 1s corresponding to Fe(III) oxide (530 eV) to a higher binding energy of 532 eV corresponding to Si(IV) oxide, was observed as shown in figure 4(*b*). Also, Si(IV) oxide peak at 103 eV is found on the Si 2p core level peak. This again supports the previous observation that Fe(0) is formed at the interface. Sputtering for a further 15 min reveals that only Fe(0) is detected and the main Si 2p peak is attributed to elemental Si(0). Figure 4(*c*) shows the corresponding atomic concentration profile for sample E. We observed a high concentration of the Cu capping layer initially as expected. As we sputter down further, a low concentration of Fe(III) oxide is observed, probably due to the diffusion of Cu into the Fe_2O_3 film. After sputtering for 6 min, we noticed the presence of metallic Fe(0) as mentioned earlier. The O 1s concentration shown represents both Fe(III) and Si(IV) oxides. Further sputtering for 10 min, shows only elemental Si(0) presence. This atomic concentration profile is similar to the analysis done for sample A where the thick Fe_2O_3 film was not capped with Cu capping layer. These results suggest that the crystalline growth of Fe_2O_3 solely depends on the difference in the enthalpy of formation of the oxides formed at the interface of Fe(III) oxide and the layer beneath it.

We have also investigated, using TEM, the interface properties of Fe_2O_3 when it is deposited directly on Si(001) substrate at 50°C. Figure 5 shows a bright field image of a cross-section of this structure. Between the Fe_2O_3 layer and the Si(001) substrate is a row of smaller grains adjacent to the Fe_2O_3 and a thin amorphous layer adjacent to the substrate. Analysis of the lattice fringe spacing of individual grains in the high resolution image of this area (figure 5(*b*)) showed that the particles adjacent to the Fe_2O_3 are metallic Fe particles with a grain size of about 5 nm. Between the Fe particles and the Si(001) substrate is an amorphous layer, which we deduce to be SiO_2.

Shown in figure 6(*a*) is the XRD pattern from Fe_2O_3 deposited directly on Si(001) substrate. We observed a peak intensity of γ-Fe_2O_3 at around 35° corresponding to (311) orientation. The corresponding XRD pattern for Fe_2O_3 deposited on Cu buffer layer is shown in figure 6(*b*). We observed a high intensity peak at 43.33° corresponding to the (400) orientation of γ-Fe_2O_3. This clearly shows that Fe_2O_3 film grown on Cu buffer layer is highly crystalline in agreement with our XPS data.

The magnetic properties of Fe_2O_3 grown on Si(001) substrate with and without a Cu buffer layer were confirmed using a VSM. Figure 7 shows the representative M–H loops for samples A and B. Sample A displayed a low coercivity of 180 Oe compared to the high coercivity value of 425 Oe for sample B, respectively. The low coercivity for sample A could be due to the presence of different phases of iron oxide at the interface which decreases the overall coercivity. However, the presence of Cu buffer layer forbids the formation of any other phase at the interface due to the high enthalpy energy of CuO, thus growing constant stoichiometric Fe_2O_3 film in sample B.

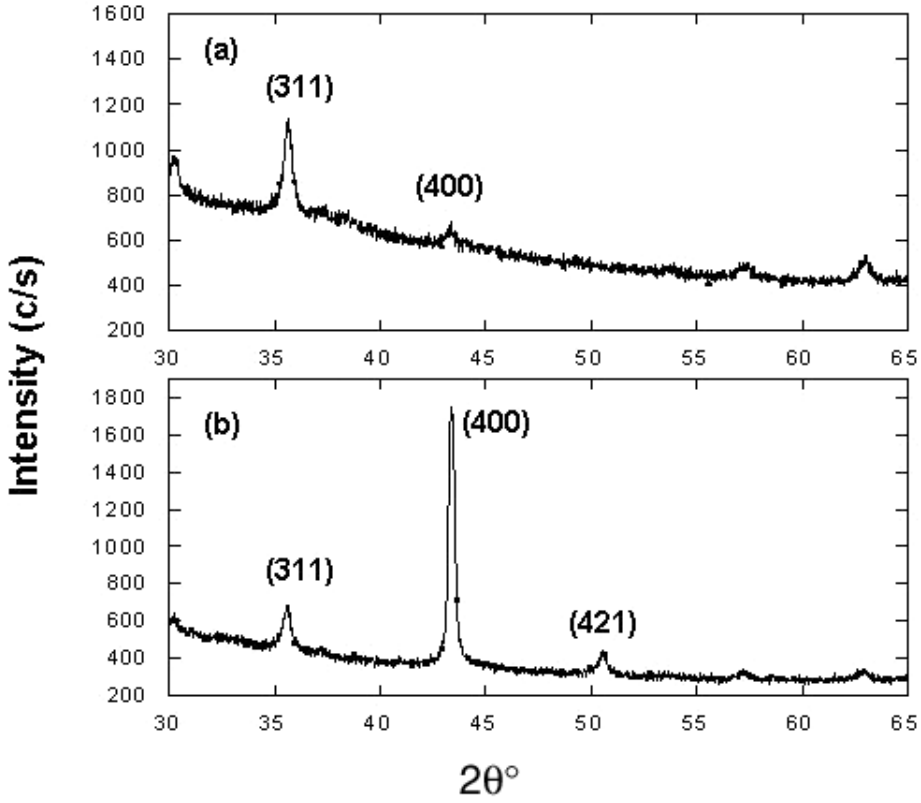

Figure 6. XRD patterns for (*a*) 200 nm of Fe_2O_3 deposited directly on a Si(001) substrate and (*b*) 200 nm of Fe_2O_3 deposited on 100 nm of Cu buffer layer.

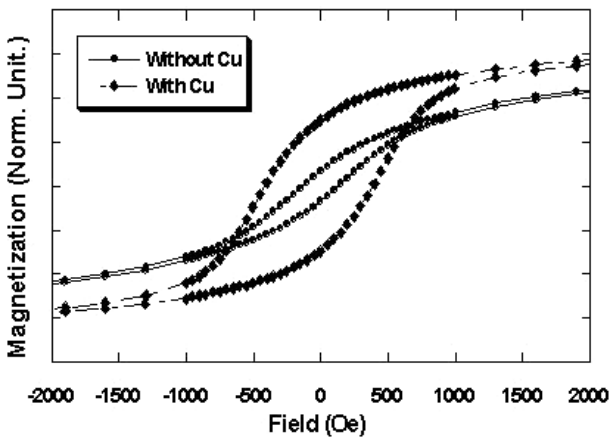

Figure 7. *M*–*H* loops for 200 nm of iron oxide film deposited on Si(001) substrate and on 100 nm Cu buffer layer.

4. Conclusion

We have investigated the interface properties of Fe_2O_3 on different templates. The enthalpy of formation of oxides is the dominant factor which determines the crystallinity of the deposited Fe_2O_3 films. For Fe_2O_3 deposited directly onto Si and on Al buffer layer, different phases of oxides were formed because the enthalpy of formation of SiO_2 and Al_2O_3 is lower than that of Fe_2O_3. Conversely, for Fe_2O_3 deposited onto a Cu buffer layer, the formation of other phases of oxide is forbidden because the enthalpy of formation for CuO is greater than that for Fe_2O_3.

Acknowledgments

This work was supported by National University of Singapore (NUS) Grant No R263-000-283-112. JS thanks NUS for her research scholarship.

References

[1] Johnson M T, Michael J R, Gilliss S R and Carter C B 1999 *Phil. Mag.* A **79** 2887
[2] Jorgenson F 1996 *The Complete Handbook of Magnetic Recording* (New York: McGraw-Hill)
[3] Jorgenson F 1993 *J. Mater. Sci. Lett.* **12** 288
[4] Kandori K, Horii I and Yasukawa A 1995 *J. Mater. Sci.* **30** 2145
[5] Ocana M, Morales M P and Serna C J 1995 *J. Colloid Interface Sci.* **171** 85
[6] Cullity B D 1972 *Introduction to Magnetic Materials* (Reading, MA: Addison-Wesley)
[7] Ye X, Lin D, Jiao Z and Zhang L 1998 *J. Phys. D: Appl. Phys.* **31** 2739
[8] Tepper T and Ross C A 2002 *J. Appl. Phys.* **97** 4453
[9] Sanders J H and Tatarchuk B J 1990 *J. Phys.: Condens. Matter* **2** 5809
[10] Chase M W 1988 *Tr. NIST-JANAF Thermochemical Tables* 4th edn *J. Phys. Chem. Ref. Data* Monograph 9